Fifth International Symposium on Marine Propulsion
SMP'17, Espoo, Finland, June 2017

Application of a BEM/RANS Interactive Method to Contra-Rotating Propellers

Yiran Su[1], Spyros A. Kinnas[2], Hannu Jukola[2]

[1] Doctoral Student, [2] Professor, Ocean Engineering Group, Department of Civil, Architectural and Environmental Engineering
The University of Texas at Austin, Austin, TX 78712, USA
[3] Steerprop Ltd. P.O. Box 217, FI-26101 Rauma, Finland

ABSTRACT

This paper introduced a BEM/RANS interactive method to predict the contra-rotating propeller (CRP) performance. In the scheme, the forward propeller and the aft propeller are handled by two separate BEM models while the interaction between them are achieved via coupling them with a RANS solver. The method provides an efficient way to predict the effective wake, the steady/unsteady propeller force, as well as other types of hydrodynamic information. The BEM/RANS method is first applied to a CRP unit in both the axisymmetric manner and the non-axisymmetric manner. The results are shown to be in good agreement with the experimental data. Finally, several other cases are tested where the podded CRP works at different steering angles.

Keywords

Contra-rotating propeller; propulsor performance; hybrid BEM/RANS method; effective wake.

1 INTRODUCTION

Contra-rotating propellers, also referred to as CRP, is a propulsion unit in which two single propellers are rotating in the opposite direction. These propellers increase the efficiency as well as reduce the propeller dimension.

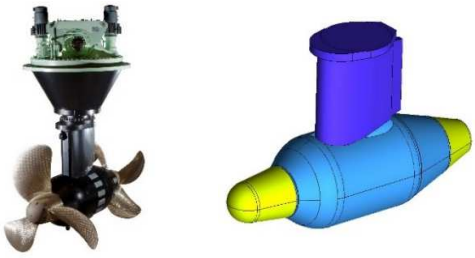

Figure 1. Photo of a CRP unit (left); CAD model of the strut and the pod (right)

To predict the CRP performance, the boundary element method (BEM), which is proved to be very successful and computationally efficient in predicting the single-propeller performance, is somewhat limited. This is due to the fact that the aft propeller is subjected to a vortical inflow which consists of both the forward propeller's trailing wake effect and the vortices caused by the boundary layer of the strut. However, the interaction between the vortical inflow and the aft-propeller-induced potential flow is beyond the capability of potential methods.

Research had been done on the prediction of the CRP performance by potential methods. Liu (2009) used a panel method to predict the steady and unsteady performance of a CRP. In this application, the interaction between the vortical inflow and the propeller induced flow is neglected so that the forward-propeller induced-velocity can be directly added to the inflow of the aft propeller. Ghassemi and Taherinasab (2013) used a similar method for CRP optimization. The same idea can also be used in the rotor-stator interaction problems for waterjet impellers (He 2010). In order to incorporate the interaction between the vortical inflow and the propeller induced flow, the vortex lattice method (VLM) can be coupled with an axisymmetric RANS solver (Gu & Kinnas 2003, Tian et al 2014). In their method, the total flow is solved by the axisymmetric RANS solver in which the propeller effects are represented by body forces (Stern et al 1988). The RANS solver is coupled with two VLM models which solve for the propeller induced flow fields for each propeller.

In this paper, a similar interactive scheme (Gu & Kinnas 2003, Tian et al 2014) is used. However, instead of predicting the mean CRP performance by coupling the steady VLM solver with an axisymmetric RANS solver, this paper focuses on both the mean and the unsteady CRP performance by coupling a boundary element solver (BEM) with either an axisymmetric RANS solver or a non-axisymmetric 3D RANS solver. The non-axisymmetric scheme enables to include the strut effect or the effect from other non-axisymmetric bodies. This is particularly important for a podded CRP because the strut may impose a strong influence to the aft propeller's inflow. Such influence may generate unsteady propeller forces and/or local cavitation. The non-axisymmetric scheme also makes it possible to consider the ship hull's effect to the CRP.

This paper starts by describing the axisymmetric and non-axisymmetric BEM/RANS interactive scheme with some discussions on the scaling factors between BEM model and the RANS model. Then the scheme will be applied to a contra-rotating propeller unit in both the axisymmetric manner (neglect the strut) and the non-axisymmetric manner (include the strut). Finally, the scheme is used to predict the CRP performance at different steering angles. Results will be analyzed.

2 METHODOLOGY

2.1 Boundary Element Method

When a propeller is operating at a low to moderate loading condition, the boundary layer on the propeller blade is thin and the flow separation is minimal. Therefore, one can assume a potential propeller induced flow without causing much numerical error. Then, the total flow U_T can be decomposed to the inflow U_{IN} (or background flow) and the propeller induced flow U_P, where the flow potential for U_P is governed by the Laplace equation. By inserting the Laplace equation into the Green's third identity, we can get the control equation for the BEM method (Fine 1992):

$$2\pi\phi = \iint_{SB}\left[\phi\frac{\partial G}{\partial \mathrm{n}} - G\frac{\partial \phi}{\partial \mathrm{n}}\right]ds + \iint_{SW}\left[\nabla\phi_w\frac{\partial G}{\partial \mathrm{n}}\right]ds \quad (1)$$

In equation (1), G is the Green's function, SB/SW are the propeller/wake surfaces, and $\nabla\phi_w$ is the dipole strength on the trailing wake which can be calculated from an iterative Kutta condition.

In the BEM solver, the inflow U_{IN} is given and used to determine the boundary condition. With the boundary condition, the above control equation can be discretized to form a linear equation system with respect to potential ϕ. Finally, U_P can be calculated. When U_{IN} is given as an axisymmetric field, only the mean performance is solved. When U_{IN} is given as a non-axisymmetric field, the propeller performance is solved for different blade angles.

2.2 RANS method

The incompressible RANS solver is often used in marine propeller applications. However, the effort for grid generation and the time for solver operations become significantly larger for contra-rotating propeller cases, especially when the unsteady interaction between the forward propeller and the aft propeller needs to be considered.

To reduce the number of cells in the RANS model, the propellers are no longer modeled by wall boundaries. Instead, they can be represented by adding local source terms into the NS equation. Since our problem is periodic, the unsteady RANS equation with source terms can be time-averaged and reduced to a steady form:

$$\frac{\partial \overline{U}_j}{\partial x_j} = Q \quad (2)$$

$$\overline{U}_j\frac{\partial \overline{U}_i}{\partial x_j} = -\frac{1}{\rho}\frac{\partial \overline{P}}{\partial x_i} + \nu\frac{\partial^2 \overline{U}_i}{\partial x_j \partial x_j} - \frac{\partial}{\partial x_j}\langle u_i u_j\rangle + \vec{F} \quad (3)$$

In this equation, $\vec{F}$ is the body force the propeller imposes to the flow and Q is the mass source which represents the blockage effect caused by the blade thickness.

2.3 BEM/RANS Interactive Scheme

In chapter 2.1, the total flow is decomposed into the inflow and the propeller induced flow. When the BEM solver is used to predict single propeller open water performance, the inflow U_{IN} is just the relative incoming velocity with respect to the propeller fixed coordinate. When the BEM solver is used to predict the propeller performance in a certain wake field, the inflow U_{IN} should be the effective wake. The effective is the nominal wake after adjusted by the propeller's influence. The purpose of the BEM/RANS interactive scheme is to efficiently evaluate the effective wake.

The effective wake U_{EFF} is defined by:

$$\vec{U}_{\mathrm{EFF}} = \vec{U}_T - \vec{U}_P \quad (4)$$

The numerical algorithm of the BEM/RANS scheme is shown in figure 2. BEM is first solved to determine the equivalent body force, the equivalent mass source, and the propeller induced velocity U_P. Then, the RANS model can be solved with the propeller effect represented by body forces and mass sources. The RANS model determines total flow U_T which leads to the effect wake according to equation (4).

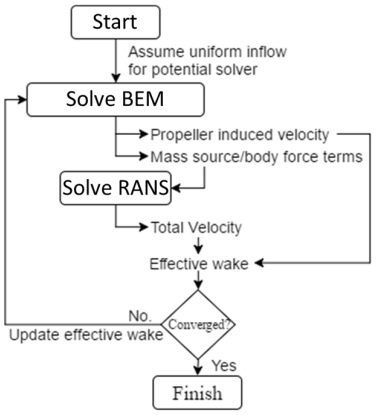

Figure 2. Numerical algorithm of the interactive scheme

In past research, to avoid singularity effects in computing the perturbation velocity, the effective wake field is often defined at an upstream disk, either a flat surface or a surface that conforms to the shape of the leading edge. In this paper, the effective wake is defined at the center of every BEM panel. In other words, the effective wake field can vary in the axial direction. According to Tian (Tian et al 2014), this can improve the numerical accuracy for various types of propellers. The details of this scheme can also be found in the work of Su and Kinnas (Su & Kinnas 2016).

Based on the purpose of an application and the level of simplification made, the scheme can be realized in either an axisymmetric manner or a non-axisymmetric manner.

In the non-axisymmetric version, a 3D steady RANS solver is coupled with an unsteady BEM solver which means the input wake U_{IN}, as well as the propeller performance, varies with the blade angle. In this case, we are able to use a steady RANS solver because, according to chapter 2.2, the unsteady RANS equation can be reduced to steady form by applying a time average over one revolving period and neglecting the crossing terms. Since the scheme is solved in a time-averaged manner, the body force field, the mass source field, and effective wake field are all time-averaged. This version of BEM/RANS scheme can be used to predict the non-axisymmetric effective wake and the unsteady propeller performances.

In the axisymmetric version of this scheme, a 2D-axisymmetric RANS solver is coupled with a steady BEM solver. In this case, the inflow U_{IN} does not change with the blade angle whlie only the mean propeller performance can be predicted. All the body force, mass source, and effective wake are averaged both in time and in θ-direction. Also, the 3D RANS equation is reduced to the 2D-axisymmetric RANS equation by averaging in the θ-direction and neglecting the crossing terms.

2.4. Application to the Contra-Rotating-Propeller

To apply this scheme to contra-rotating propellers (CRP), the RANS solver should be coupled with two BEM models: one model is for the forward propeller and the other model is for the aft propeller.

Both BEM and RANS are solved with dimensionless values. The BEM solver is nondimensionalized by the propeller maximum radius and the RANS solver is nondimensionalized by the forward propeller maximum radius. Because the aft propeller has a smaller radius than the forward propeller, the aft propeller BEM model has a different scaling factor. Therefore, both the coordinates and the body force/ mass source need to be scaled when the aft propeller BEM model is coupled with the RANS solver. The geometric scaling factor m is defined by equation (5) where R_f and R_a are the maximum radius for forward and aft propeller in real dimension.

$$m = \frac{R_f}{R_a} \tag{5}$$

Then, the scaling of the body force F and mass source Q are shown in equation (6) - (9).

$$\frac{F_{RANS}}{\rho V_S^2/R_{RANS}} = \frac{F_{BEM}}{\rho V_S^2/R_{BEM}} \tag{6}$$

$$\frac{Q_{RANS}}{\rho V_S/R_{RANS}} = \frac{Q_{BEM}}{\rho V_S/R_{BEM}} \tag{7}$$

$$F_{RANS} = \frac{R_{BEM}}{R_{RANS}} F_{BEM} = mF_{BEM} \tag{8}$$

$$Q_{RANS} = \frac{R_{BEM}}{R_{RANS}} Q_{BEM} = mQ_{BEM} \tag{9}$$

3 NUMERICAL MODELS

In this paper, the BEM/RANS method is applied to a CRP unit via three different models: an axisymmetric model which neglect the effect of the strut and effect from all other non-axisymmetric bodies, a non-axisymmetric model which includes the strut effect via RANS, and finally a non-axisymmetric model with different steering angles.

3.1 Axisymmetric model

In this application, a 2D-axisymmetric RANS model, as shown in figure 3a, is coupled with two BEM models, as shown in figure 3b and 3c. The strut is neglected in this model. A k-ω SST turbulent viscosity model is used in the RANS solver and the body force/mass source zone is marked in figure 3a. The inflow boundary of the RANS model is given by the ship speed V_S (1m/s). With a 2.7 GHz E5-2680 processor, it takes about 1 hours for the interactive scheme to converge. It is worth noting that both the forward propeller and the aft propeller are solved as right-handed propellers in BEM. The θ-component of the body force and the effective wake are reversed within the intermediate step between the BEM solver and the RANS solver.

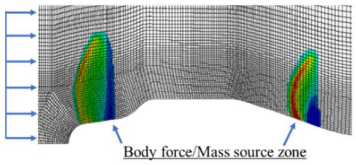

(a) Axisymmetric RANS model (outer boundary not shown)

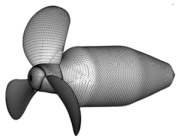

(b) BEM model (forward)

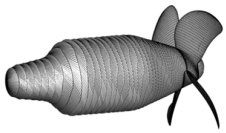

(c) BEM model (aft)

Figure 3. Axisymmetric BEM/RANS model

3.2 Non-axisymmetric model

In this application, a 3D RANS model, as shown in figure 4, is coupled with two BEM models, as shown in figure 3b and 3c. In the RANS model, the strut and the pod are represented by non-slip walls while the free surface is simplified to a symmetry boundary condition. With four 2.7 GHz E5-2680 processor, it takes around 5 hours for the interactive scheme to converge.

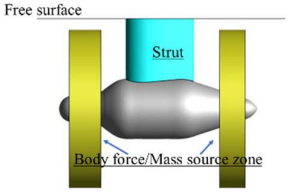

Figure 4. Non-axisymmetric RANS model (outer boundary is not shown in the left figure)

3.3 Non-axisymmetric model with inclined shaft

As a podded contra-rotating propeller, this CRP unit is able to rotate around the vertical axis. Therefore, it is also important to predict the propeller performance when the shaft is not parallel to the incoming flow direction.

In this application, several different steering angles φ are used, ranging from -10 degrees to +10 degrees. The model set up is almost the same as in chapter 3.2. In the RANS model, instead of rotating body force zone, the inflow is given at an inclined angle.

4 RESULTS AND COMPARISON

In this paper, all the dimensionless numbers are defined based on the forward propeller diameter D_F, ship speed V_S, and the propeller rpm n. The advance radio J_S, thrust coefficient K_T, and torque coefficient K_Q are defined by equation (10).

$$J_S = \frac{V_s}{nD_F} \qquad K_T = \frac{T}{\rho n^2 D_F^4} \qquad K_Q = \frac{T}{\rho n^2 D_F^5} \tag{10}$$

Figure 5 shows the unsteady propeller KT and KQ history in different iterations. At the first iteration, both the axisymmetric case (left) and the non-axisymmetric case (right) assume a uniform inflow and get constant propeller forces over the time (blade angle). From the second iteration, the forces on both the forward and aft propellers begin to change due to the influence from the other propeller, from the strut, and from the free surface. The last two influences only exist in the non-axisymmetric model. With a moderate relaxation factor, the scheme converges at around the 5th iteration. For both cases, the aft propeller is more affected by the interaction than the forward propeller. The converged result from axisymmetric case remains constant over time while the non-axisymmetric case developed some unsteady component.

Figure 6 compared the propeller thrust and torque with experiments at zero steering angle. The forces are given by total unit, as well as by individual propeller. It is worth noting that the total thrust also includes the negative drag force on the pod/strut. As is shown in the figure, the results of the BEM/RANS interactive scheme have a good agreement with the experimental value. Both the axisymmetric case and the non-axisymmetric case behave well at a wide range of advance ratios near the design load condition. As the propeller loading is higher, the error becomes more obvious. This might be caused by the higher viscous effects from the thicker boundary layer at the blade suction side.

Figure 7 is a typical body force/mass source distribution at the propeller zone when the CRP unit is working at a zero-steering-angle. The forward propeller and the aft propeller both generate a positive axial body force onto the flow while they impose circumferential body force at opposite directions. The mass source is mostly determined by the gradient of the blade thickness in the flow direction; a volume integration of the mass source should lead to a zero value. Figure 8 shows the axial and swirl components of the total velocity U_T/V_S on the centerline plane as well as the axial component of the total velocity at a station in the middle between the strut trailing edge and the aft propeller leading edge. As shown in the second figure, the swirl component of the flow induced by the forward propeller is mostly decelerated by the aft propeller except for very low radius regions. The boundary layer effect of the strut can also be observed on third figure.

It is also useful to predict the forces generated by the CRP unit when it is working at a steering angle. To simplify the problem, the wake flow associated with the turning ship hull is not considered and the interactions between multiple CRP units are neglected. In other words, a single CRP unit is working in the open water with an inclined pod. To solve this problem, the non-axisymmetric version of the BEM/RANS scheme is needed. The predicted forces generated by the CRP unit at different steering angles are shown in figure 9. The left figure includes value of the total force in four different directions, all of which are non-dimensionalized by $\rho n^2 D_F^4$. Force K_{HX} and K_{HS} are forces in the longitudinal direction and the horizontal direction of the ship hull coordinate system. Force K_{PX} and K_{PS} are forces in the axial direction and the horizontal direction of the propeller coordinate system. Both horizontal forces point from port side to the starboard side and K_{PX} is the same as the propeller's thrust coefficient. The right figure shows the contribution of the thrust coefficients from the forward propeller and the aft propeller.

Figure 10 shows axial component of the total velocity on the horizontal plane that passes the mid-span of the strut. In figure 11, the effective wake of the aft propeller is plotted on the propeller disk surface. The axial velocity is represented by the color while the in-plane velocity components are given by arrows. Because the effective wake in this scheme is a 3D flow field, figure 11 is actually showing a reduced-dimension effective wake which is averaged in the propeller chordwise direction.

As shown in figure 9 (left), as the propeller steering angle increases, force K_{HX} remains nearly constant while force K_{HS} behaves linear to the steering angle. In the propeller coordinate system, the horizontal force increases with the steering angle while the axial force remains nearly constant. If we look at the contributions from the forward propeller and from the aft propeller, as show in figure 9 (right), it can be found that the forward propeller's axial force keeps almost unchanged with the steering angle while the aft propeller's axial force decrease with the steering angle. This can be explained by the struct effect. The aft propeller is working under the effect from the forward propeller's trailing wake which includes an axial velocity and a swirl velocity, as shown in figure 10 and 11. When a ±10 steering angle is given, depending on the sign of the angle, the swirl component of the effective wake is either strengthened or weakened. This leads to the monotonic trend between the steering angle and the aft axial force.

Figure 11 shows the aft propeller effective wake at the mid-cord disk. With a ±10 steering angle, part of the aft propeller falls outside of the forward propeller's trailing wake region. The cavitation behavior of the aft propeller in such situations will be studied in the future.

In a more realistic case, the wake flow from the hull, as well as the rotating motion can be included in both the RANS solver and BEM solver by the effective wake.

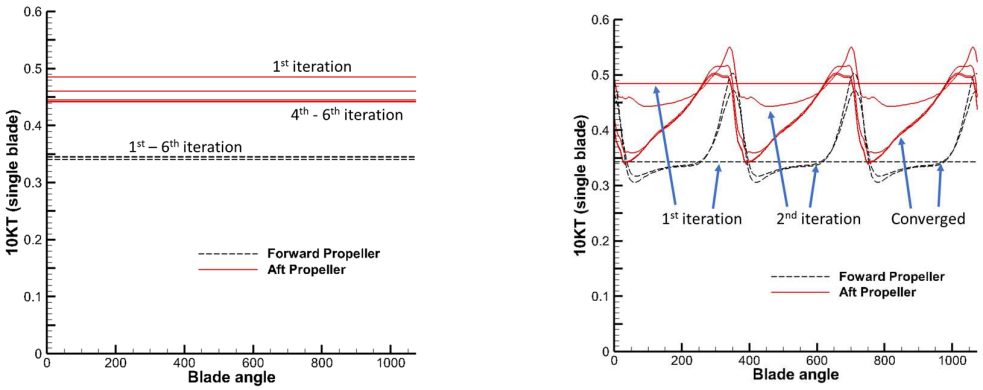

(Axisymmetric case) (Non-axisymmetric case)

Figure 5. Convergence history of the unsteady propeller thrust coefficients.

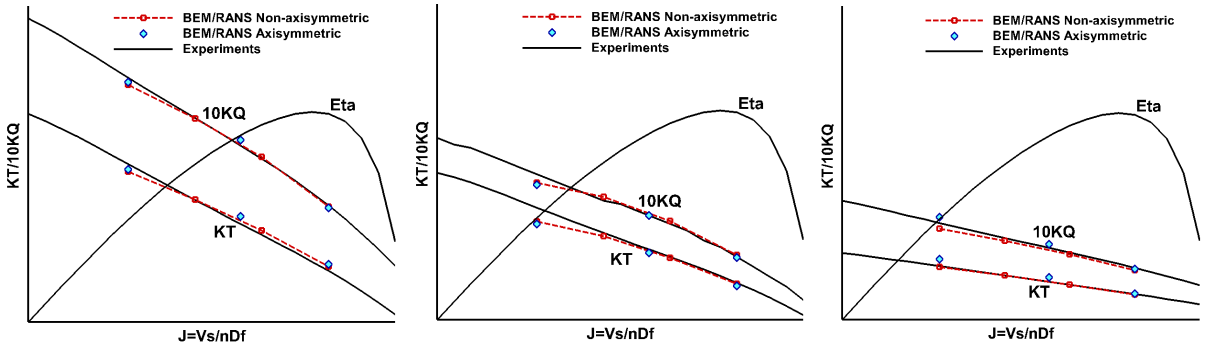

(Total) (Forward propeller) (Aft propeller)

Figure 6. Comparison of propeller thrust/torque coefficients between BEM/RANS results and experimental data.

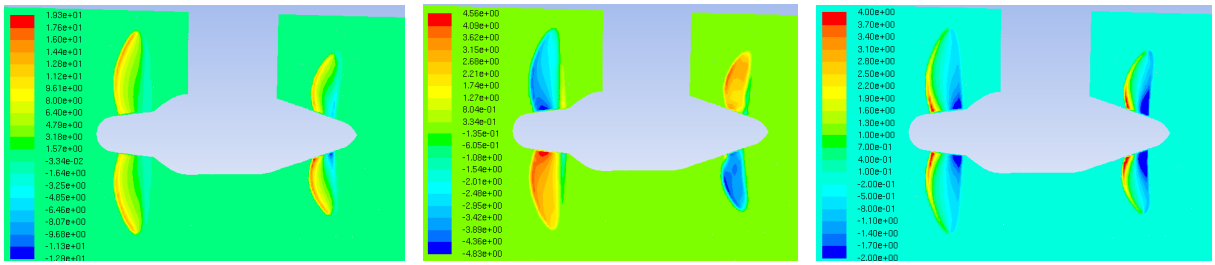

(Axial body force) (Z-body force) (Mass source)

Figure 7. Body force/mass source distribution in the non-axisymmetric BEM/RANS model.

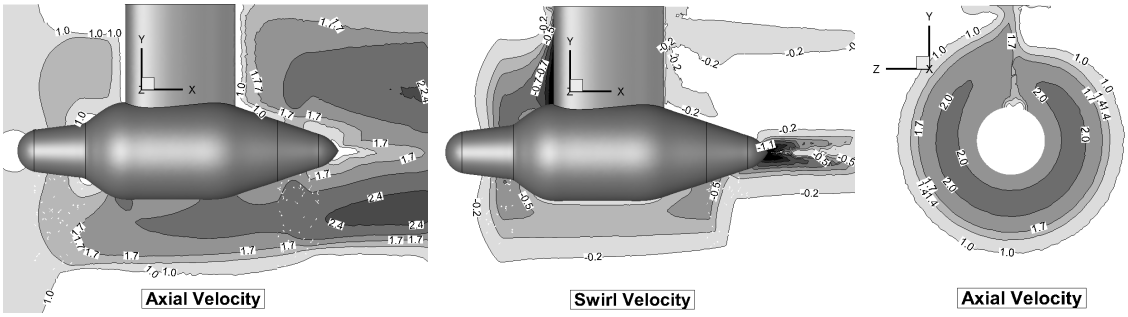

Figure 8. Total velocity U_T distribution on the centerline plane (left, middle); total velocity U_T distribution on the station between the strut trailing edge and the aft propeller leading edge (right).

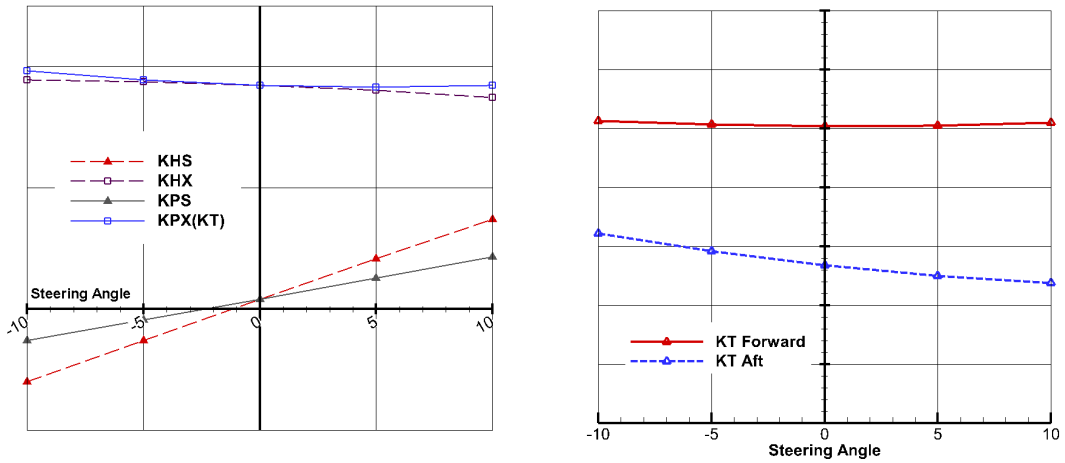

Figure 9. Propeller total steering forces (left) and individual thrust/torque coefficients (right) at different steering angles.

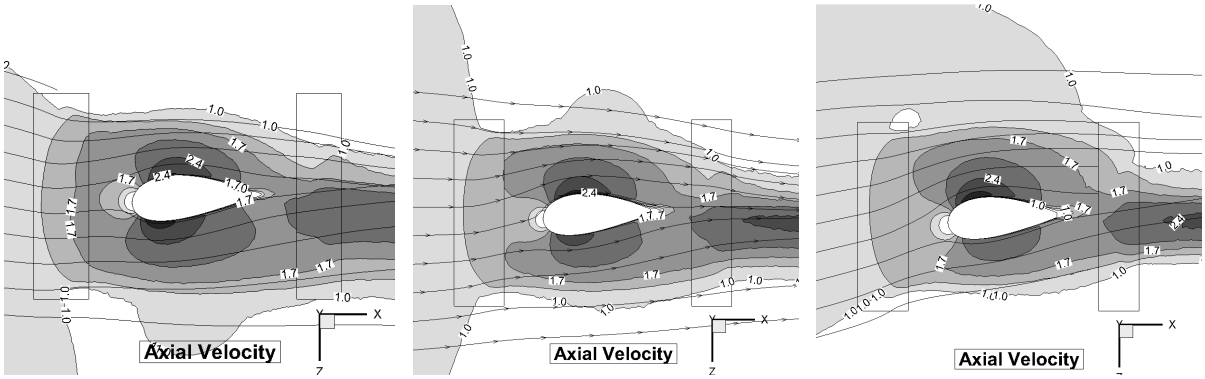

(-10 degree steering angle) (0 degree steering angle) (+10 degree steering angle)

Figure 10. Total velocity U_T distribution on the waterline plane near the half span of the strut.

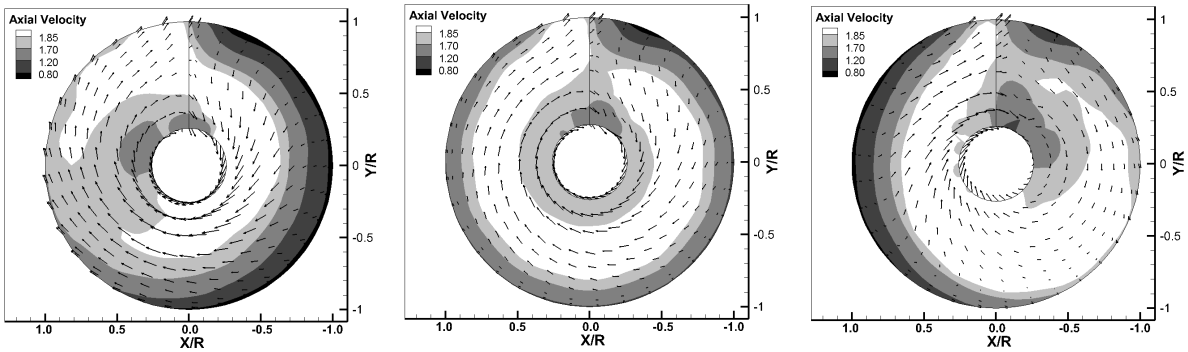

(-10 degree steering angle) (0 degree steering angle) (+10 degree steering angle)

Figure 11. Effective wake field of the aft propeller at different steering angles. The wake field is only plotted on the mid-cord disk of the aft propeller. It may vary along the axial direction.

5 CONCLUSIONS AND FUTURE WORK

In this paper, a BEM/RANS interactive scheme is applied to the contra-rotating-propeller (CRP) cases. In this scheme, the propeller performance is solved by the BEM model while the forward-aft propeller interaction is included in a time-averaged sense via the RANS solver. The method was used on a CRP unit in both the axisymmetric manner and the non-axisymmetric manner. Results show good agreement with open water model test results. Then, the method is applied to the same CRP unit, but with different steering angles.

The result shows that both the axisymmetric scheme and the non-axisymmetric scheme behave well in terms of predicting the mean open-water propeller performance, while the non-axisymmetric scheme is able to handle more complicated inflows.

Future work includes considering the ship motion as well as the hull wake in the steering case, which makes it closer to the real steering situation. Then, the unsteady effects can be included in this scheme by coupling the BEM solver with an unsteady RANS solver via time-dependent body forces and time-dependent effective wake fields. The method can also be applied to evaluate the interaction between multiple CRP units. Finally, the computational efficiency can be improved by replacing the propeller body force with an immersed boundary in the RANS solver.

ACKNOWLEDGMENTS

Support for this research was provided by the U.S. Office of Naval Research (Grant No. N00014-14-1-0303; Dr. Ki-Han Kim) and Phase VII of the "Consortium on Cavitation Performance of High Speed Propulsors" with the following members: Kawasaki Heavy Industry Ltd., Rolls-Royce Marine AB, Rolls-Royce Marine AS, SSPA Sweden AB, Andritz Hydro GmbH, Wärtsilä Netherlands B.V., Wärtsilä Norway AS, Wärtsilä CME Zhenjiang Propeller Co. Ltd., and Steerprop Ltd.

REFERENCES

Fine, N. E. (1992). 'Nonlinear analysis of cavitating propellers in nonuniform flow'. Ph.D. dissertation, Massachusetts Institute of Technology Cambridge Department of Ocean Engineering.

Gu, H. & Kinnas, S. A. (2003). 'Modeling of contra-rotating and ducted propellers via coupling of a vortex-lattice with a finite volume method'. Proceedings of Propeller/Shafting 2003 Symposium, SNAME, Virginia Beach, USA.

Ghassemi, H., Taherinasab, M. (2013). 'Numerical calculations of the hydrodynamic performance of the contra-rotating propeller (CRP) for high-speed vehicle'. Polish Maritime Research. 20, no. 2: 13-20.

He, L. (2010). 'Numerical simulation of unsteady rotor/stator interaction and application to propeller/rudder combination'. Ph.D. dissertation, Ocean Engineering Group, CAEE, the University of Texas at Austin.

Liu, X. L. (2009). 'A potential based panel method for prediction of steady and unsteady performances of contra-rotating propellers'. Proceedings of the first International Symposium on Marine Propulsors, Trondheim, Norway.

Stern, F., Kim, H., Patel, V., & Chen, H. A. (1988). 'Viscous-flow approach to the computation of propeller-hull interaction'. Journal of Ship Research, 32, 4, 246-262.

Su, Y. & Kinnas, S. A. (2016). 'A Generalized Potential / RANS Interactive Method for the Prediction of Propulsor Performance'. In Proceedings of SNAME maritime convention.

Tian, Y., Jeon, C. H., & Kinnas, S. A. (2014). 'Effective Wake Calculation/Application to Ducted Propellers'. Journal of Ship Research, Vol. 58, No. 2, June 2014, pp. 1–13.